sciendo

Strojnícky časopis – *Journal of* MECHANICAL ENGINEERING,
VOL 69 (2019), NO 4, 65 - 88

STU SjF

GREY-WPCA BASED PARAMETRIC-OPTIMIZATION AND MODELLING OF CHROMIUM POWDER MIXED SURFACE-ELECTRO DISCHARGE DIAMOND GRINDING OF INCONEL 600 USING RSM

MANOJ Modi[1], GOPAL Agarwal[2], SWATI D Chaugaonkar[3]

[1]Acropolis Institute of Technology and Research, Department of Mechanical Engineering, Indore, India, e - mail: manojmnitjaipur1@gmail.com
[2]Malaviya National Institute of Technology, Department of Mechanical Engineering, Jaipur, Rajasthan, India, e - mail: agrawal.drg@gmail.com
[3]Shri Govindram Seksaria Institute of Technology and Science, Department of Mechanical Engineering, Indore, Madhya Pradesh, India, e - mail: swati18may@yahoo.co.in

Abstract: The PMS-EDDG is an effective hybrid process to beat the problems identified in machining of Inconel 600 through the conventional machining process. This hybrid-machining-process is a combination of S-DG and Powder Mixed-EDM process. Modeling, comparative investigation, determination of optimal setting of process factors, and various surface developments in S-EDDG of Inconel 600 with chromium and absence of chromium-powder blended dielectric fluid (DF) have been narrated in this research work. One set of 31 experiments with chromium-powder and another set of 31 experiments without chromium-powder mixed DF was conducted on this set-up in accordance with the C-C-R-D plan of experimentation. The developed models through RSM support to investigate the behavior of input process-factors over the responses. The input factors in this research work are ampere-current (I), pulse-on-time (T_{on}), wheel speed (WS), and duty cycle (DC). The MRR and R_a are the output-responses in this machining process. The optimum setting of process-parameters is computed through the integrated Grey-Taguchi based WPCA-approach. The confirmation experiment is conducted on this set-up at the optimum-condition and its results display the agreeable matching among the actual and predicted values. The WMPI is improved by 0.414. The SEM investigation has been conducted at the optimum-condition on the produced machined-surfaces and on the produced white recast-layer thickness.

KEYWORDS: Analysis of variance (ANOVA); Powder Mixed Surface-Electro Diamond Discharge Grinding (PMS-EDDG); hybrid process; RSM; and Inconel 600.

1 Introduction

There are diverse applications in which Ni-based super-alloys are utilized adequately i.e. in aircraft, turbine components, nuclear reactor parts and in petrochemical equipments etc. as it has excellent properties like high strength, creep resistance, fatigue resistance at high temperature [1]. Ni-based Inconel 718 is difficult to machine material with conventional machining due to its higher hardness, toughness and less thermal conductivity [2]. This is why advanced hybrid machining process based on thermo-electric energy and mechanical energy is adopted here for ease machining of Inconel 600. Luo et al. [3] did the experimental work on ED-Machining of Chromium-12 steel and narrated that discharge transitivity in IEG relies upon the gap debris. They also described that debris not only supports in ignition process but also responsible for enhance the gap-size. Ho et al. [4] reported about the research trends in ED-Machining to raise the performance estimates, and optimization of process factors. They also reported the scope of ED-Machining uses is featured along with the advancement of HM-processes. Lee et al. [5] conducted the experiments on ED-Machining with D-2 and H-13 tool steels. They reported an investigation about the connection among the ED-Machining factors

DOI: 10.2478/scjme-2019-0044, Print ISSN 0039-2472, On-line ISSN 2450-5471

and surface-cracks by utilizing the factorial-design, based on the T_{on}, and ampere-current factors. Kao et al. [6] performed the experiments and narrated that Grey-TM integrated methodology improves the multi-output-characteristics of the process in ED-Machining of Ti-6Al-4V. Tzeng et al. [7] did experimental work on ED-Machining with SKD-11 steel. They choose aluminum, chromium, copper, and silicon-carbide powders for this work and observed that aluminum powder make the greatest gap size, trailed by Cr, than Si-C and with Cu has the lowest gap size. George et al. [8] utilized the TM technique to determine the optimal setting of process factors in ED-Machining of Carbon-Carbon composite. Modi et al. [9] utilized DA technique for the development of MRR, and SR models in hole-drilling operational work on PM-ED Machining. He also investigated the impact of process factors on the process outcomes. Singh et al. [10] conducted experiments and utilized Grey-TM method for multi-output optimization of process factors in F-EDDG with Tungsten Carbide-Co composite-work material. Gauri et al. [11] utilized various multi-response optimization methodologies on W-ED Machining data sets and also distinguished the performance obtained from these methodologies. Lin et al. [12] utilized Grey-Fuzzy technique for multi-response optimization of process factors in ED-Machining with SKD-11 steel. Modi et al. [13] described the details of PMEDM with grinding attachment process and determined the optimum setting of process parameters through WPCA method. Modi et al. [14] did the experiments on EDDSG with Ti6AL4V. They reported that Grey-TM methodology enhances the machining performance. Chen et al. [15] performed the experimental work on ED-Machining of Ti6Al4V work material with distilled water and with kerosene. They also reported about the material removal mechanism in distilled water and in kerosene. Liao et al. [16] clarified that there are a few weaknesses in PCA procedure. He utilized WPC Approach to beat these inadequacies and used this technique for multi-response-optimization. Kumar et al. [17] conducted the experiment on various titanium alloys in PMED-M process and study the effect of cryogenic treatment on TWR. He also developed the model of TWR by using DA. Ramesh et al. [18] did experimental work on PBED-Machining of AISI P-20 steel. They reported that the impact of various powders and diverse electrode materials on PBED-M process performance. Modi et al. [19] conducted the experiments on EDDSG with Ti6Al4V and reported that the effect of input parameters on the output response. Modi et al. [20] performed the tests on EDDS-G with titanium alloy and repoted that the influence of dielectric jet flushing on the responses. Kumar et al. [21] conducted experiments on PMED-Machining of Inconel 800 and utilized RSM technique for the development of MRR and TW-R models. They utilized desirability technique for multi-response optimization of process factors. Modi et al. [22] conducted the experiments on lathe with HSS and utilized the Taguchi's method for modeling and optimization of machining parameters. Modi et al. [23] did the experiments on drilling machine with Al-SiC composite and utilized Taguchi's Method to determine the optimum setting of process parameters. Prakash et al. [24] performed the experimental work on PMED-Machining of Ti35Nb7Ta5Zrβ-Ti alloy with silicon powder blended DF. They observed that PAED-Machining enhance the process-performance. Razak et al. [25] did the experimental work on PMED-Machining of Mg-alloy and revealed that Zn blended DF alters the rate of corrosion of Mg-alloy. Modi et al. [26] did the experimental work on PMEDM with Nimonic 80A with Al, and Cr powder mixed dielectric fluid. They reported that effectiveness of ED Machining is influenced by the properties of added powders in dielectric fluid. Modi et al. [27] performed the tests on EDDS-G of titanium alloy with SiC powder mixed DF. They applied integrated multi-output optimization methodology to determine the optimum setting of process variables and reported that the integrated statistical methodology enhances the multi-output performance index by 0.375. De et al. [28] conducted the tests on WEDM with sintered titanium. They studied the effect of various parameters i.e., pulse on time, pulse off time, wire feed, and wire tension on MRR, SR, kerf width, and over cut. They applied RSM for the development of mathematical model of the responses. Raturi et al. [29] did the tests on WEDM with Al 6063/SiC/Al2O3 composite. They reported that the MRR and SR increase with increase in % weight fraction of SiC and Al2O3 particles in MMCs and HMMCs. Umacharan et al. [30] did experimental work on electro discharge-diamond-drilling with nimonic-alloy and utilized GRA-PCA technique for multi-objective-optimization of process factors. H-M-P performance is more adequate than the individual performance of adjoining process with same input factors [31, 32].

Based on the literature review, the surface grinding of Inconel 600 in S-EDDG process with chromium and absence of chromium powder blended with dielectric-fluid is the field under development. The aim of this work is to thorough investigate the mechanism of machining of Inconel 600 utilizing the PMS-EDDG process, formulate the empirical models of the process-responses with chromium and absence of chromium powder blended with DF in S-EDDG of Inconel 600, comparative study to analyze the behaviour of input process factors against the process-responses, determination of optimum condition of process parameters with Cr powder mixed dielectric fluid by utilizing integrated Grey-TM based WPCA method, and finally examine the effect of presence and absence of chromium powder in dielectric fluid on S-EDDG produced surfaces and on the WRL thickness at the optimum condition.

To fulfil these aims, one-set of 31 experiments with chromium powder and another set of 31 experiments without Cr powder blended dielectric fluid were conducted on S-EDDG set-up. The mathematical models of the responses were developed using the RSM. These developed empirical models have been utilized to study and compare the behaviour of input process factors against the responses with chromium and absence of chromium powder blended DF. TM is not fit for multi-response optimization of process factors in PMS-EDDG of Inconel 600. This is why the Grey-TM based WPCA approach has been utilized for the determination of the optimum combination of machining variables with chromium powder blended DF in S-EDDG of Inconel 600. This integrated optimization approach suggested an optimum setting of process parameters which helps the engineer to develop a cost-effective process. The SEM investigations have been conducted to study the effect of presence and absence of Cr powder in the dielectric fluid on S-EDDG produced surfaces and on the WRL thickness.

2 Experimental-Procedure with PMS-EDDG process

Two sets of thirty-one experiments were conducted in accordance to Central-Composite-Rotary-Design plan of experimentation on in-house composed and created PMS-EDDG frame-up with Inconel 600 work-piece. The illustrative drawing and photographic image of PMS-EDDG set-up is displayed in “Figs. 1 and 2” respectively. The thirty-one tests were conducted on this frame-up with chromium powder blended DF. Another set of thirty-one experimentations was conducted on the same frame-up without chromium powder blended DF. The input factors associated with this research work were ampere-current, T_{on}, S, and duty-cycle.

Contingent on starting test outcomes and ED-Machining limit, the levels of factors were picked as depicted in Table 1. The chromium powder concentration was taken 3 gram/ litre in the dielectric fluid. The Inconel 600 was chosen as the work-material which is rectangular and flat in shape. The structure of Inconel 600 work-material is Nickel, Cr = 15 %, Fe = 8 %, V = 3.7 %, C = 0.15 %, Mn = 1 %, S = 0.015 %, Si = 0.5% and Cu= 0.5 %. The size of the work-piece is 60 mm x 10 mm x 10 mm.

The “Eq. (1)” was utilized to compute the MRR (mm^3/minute).

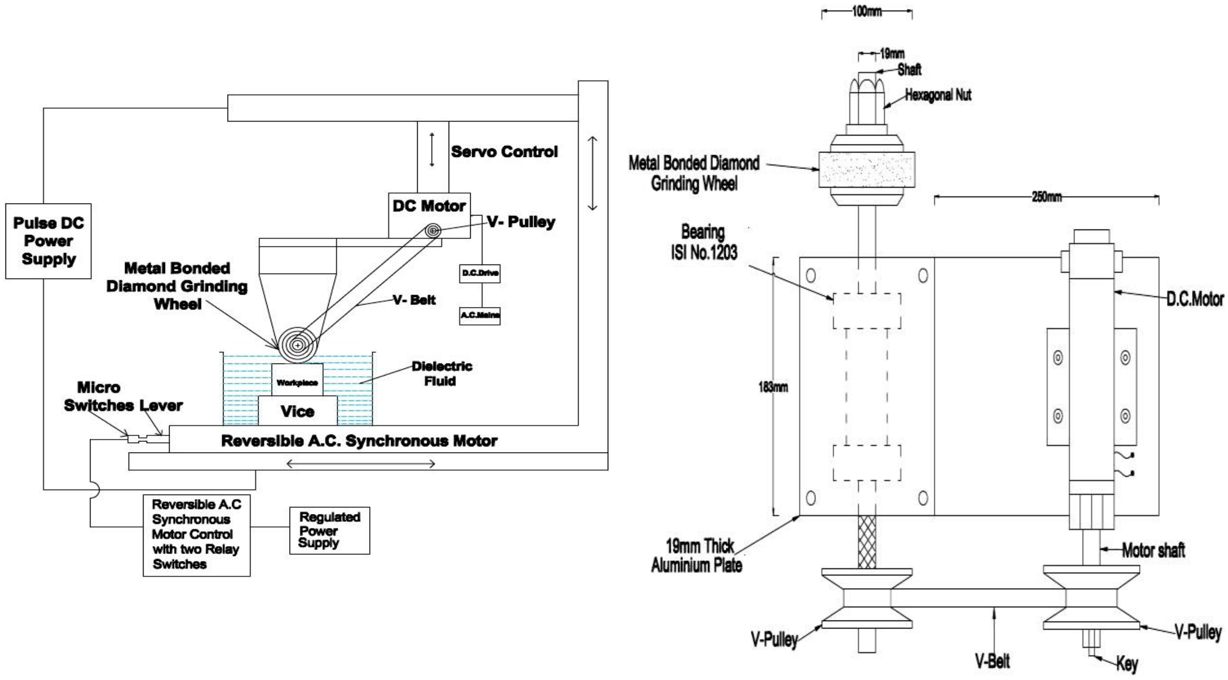

Fig. 1. Illustrative drawing of PMS-EDDG attachment.

Fig. 2. Photographic image of PMS-EDDG attachment.

$$MRR\left(mm^3/minute\right)=\frac{Difference\ in\ weight\ of\ w/p\ before\ and\ after\ the\ machining \times 1000}{t \times \rho} \quad (1)$$

The machining time (t) in this process is equal to 60 minutes; the density of the work piece material (ρ) is equal to 8.47 gm/cm^3. The electronic balance was used for the measurement of weight. The Surtronic-25 SR analyzer at a cut-off estimation of 0.8 mm was utilized for the estimation of R_a. The advanced tachometer was utilized for measurement of wheel-speed. The content of bronze G-wheel diamond bonded is listed in Table 2.

Table 1. Input machining factors involved in this experimental work and its range

Parameters	-2	-1	0	+1	+2
Current (I)	1	3	5	7	9
Pulse-on-time (T_{on})	100	125	150	175	200
Wheel-Speed (S)	200	400	600	800	1000
Duty-Cycle (DC)	0.61	0.65	0.69	0.73	0.77

Table 2. Content of bronze G-wheel diamond bonded

Abrasive	Diameter in mm	Thickness in mm	Bond Material	Concentration %	Bore in mm	Depth of abrasive in mm	Grit size
Diamond	100	10	Bronze	80	32	5	80/100

3 Response Surface Modeling (RSM)

RSM is an accumulation of statistical and mathematical methodologies. This methodology is applied to acquire the connection among the factors associated with machining process and the process-responses in PMS-EDDG of Inconel 600 with chromium and absence of chromium powder blended DF [23].

The "Eq. (2)" is used to express the surface-response.

$$Y = a_0 + \sum_{i=1}^{n} a_i x_i + \sum_{i=1}^{n} a_{ii} x_i^2 + \sum_{j>i} a_{ij} x_i x_j \qquad (2)$$

Here, Y = Output Responses, a_o= Free-terms coefficient, a_i= Linear-terms coefficient, a_{ii}= Quadratic-terms coefficient, and a_{ij} = Interaction-terms coefficient.

4 Mathematical Modelling of Experimental Responses with Cr powder mixed dielectric-fluid

The first set of thirty-one experiments was conducted on S-EDDG of Inconel 600 with chromium powder blended DF. The estimation of all the factors associated with this experimentation work is displayed in Table 1.The C-C-R-D experimentation plan is depicted in Table 3. This C-C-R-D design consist of sixteen corner points at the interval of [-1, 1], Eight axial points at the interval of [-2, 2], and the central point at zero level reiterate seven times. This includes the total 31 experimental runs. The 'Design Expert 8.0.7.1' [33] was used for the development of mathematical models of MRR and R_a. After removal of non-valuable terms, the numerical models of MRR and R_a are depicted by the "Eqs. (3) and (4)".

$$MRR = 0.46 + 0.14I + 0.058T_{on} + 0.058S - 0.032DC + 0.028I^2 \qquad (3)$$

$$\boldsymbol{R_a = 4.22 + 0.54I + 0.23T_{on} - 0.26S + 0.61DC - 0.076T_{on}^2} \qquad (4)$$

The different graphs were plotted to forecast the behavior of input process factors against the process outcomes utilizing the "Eqs. (3) and (4)".

4.1 ANOVA analysis for MRR and R_a model

The ANOVA-outcomes for the MRR and R_a are depicted in Tables 4 and 5 respectively. "Figs. 3 and 4" display the N % probability graph of the residuals for MRR and R_a respectively and demonstrate that residuals scatter around the straight-line exhibiting that errors are N-distributed [34]. Moreover, from the "Figs. 5 and 6", it was noticed that the predicted values from the empirical model were seen to be in excellent matching with the actual values for MRR and R_a. The F-value of MRR and R_a model with chromium powder blended DF is 300.63 and 203.27 respectively with value of $p < 0.0001$ for both the models so that these developed empirical equations of MRR and R_a are adequate to depict the association among input machining variables and the output-responses. The R-squared values for MRR and R_a model is 0.9836 and 0.9760 respectively, that indicates the developed models are significant in describing the variation of MRR and R_a up-to 98.36 % and 97.60 %. There is negligible difference between Adj R-Squared and Pred R-Squared value for both the models. The values of CV are 4.43 and 3.28 for MRR and R_a model respectively. As the value of CV becomes smaller, it will indicate towards enhanced precision and consistency of experiments performed. The Adeq-Precision value for both the models is essentially higher than the required-one and hence indicates an adequate signal for both the models.

Table 3. C-C-R-D experimental-plan and process-responses with Cr powder blended DF

Exp. Number	Current (I) ampere	Pulse-on-time (T_{on}) µs	Wheel Speed (S) RPM	Duty Cycle (DC)	MRR (mm^3/min) Experimental	MRR (mm^3/min) Predicted	R_a (µm) Experimental	R_a (µm) Predicted
1	-1	-1	-1	-1	0.279	0.264	3.21	3.024
2	1	-1	-1	-1	0.531	0.544	4.06	4.104
3	-1	1	-1	-1	0.370	0.380	3.36	3.484
4	1	1	-1	-1	0.642	0.660	4.49	4.564
5	-1	-1	1	-1	0.368	0.380	2.58	2.504
6	1	-1	1	-1	0.644	0.660	3.42	3.584
7	-1	1	1	-1	0.494	0.496	3.04	2.964
8	1	1	1	-1	0.768	0.776	4.05	4.044
9	-1	-1	-1	1	0.198	0.200	4.35	4.244
10	1	-1	-1	1	0.464	0.480	5.47	5.324
11	-1	1	-1	1	0.305	0.316	4.69	4.704
12	1	1	-1	1	0.589	0.596	5.99	5.784
13	-1	-1	1	1	0.321	0.316	3.73	3.724
14	1	-1	1	1	0.598	0.596	4.76	4.804
15	-1	1	1	1	0.419	0.432	4.32	4.184
16	1	1	1	1	0.712	0.712	5.38	5.264
17	-2	0	0	0	0.289	0.292	2.89	3.140
18	2	0	0	0	0.858	0.852	5.17	5.300
19	0	-2	0	0	0.360	0.344	3.38	3.456
20	0	2	0	0	0.605	0.576	4.30	4.376
21	0	0	-2	0	0.323	0.344	4.81	4.740
22	0	0	2	0	0.542	0.576	3.82	3.700
23	0	0	0	-2	0.531	0.524	3.26	3.000
24	0	0	0	2	0.389	0.396	5.29	5.440
25	0	0	0	0	0.457	0.460	4.16	4.220
26	0	0	0	0	0.511	0.460	4.17	4.220
27	0	0	0	0	0.436	0.460	4.24	4.220
28	0	0	0	0	0.455	0.460	4.14	4.220
29	0	0	0	0	0.462	0.460	4.08	4.220
30	0	0	0	0	0.478	0.460	4.07	4.220
31	0	0	0	0	0.401	0.460	4.29	4.220

5 Mathematical Modelling of Experimental Responses without Cr powder mixed dielectric-fluid

The second set of thirty-one experiments was conducted on S-EDDG of Inconel 600 without chromium powder blended DF. The estimation of all the factors related with this experimentation work is displayed in Table 1. The C-C-R-D experimentation plan is depicted in Table 6. The 'Design Expert 8.0.7.1' [23] was used for the development of mathematical models of MRR and R_a in S-EDDG of Inconel 600 without chromium powder mixed dielectric fluid. After elimination of non-valuable terms, the mathematical models of MRR and R_a are depicted by the "Eqs. (5) and (6)".

$$MRR = 0.42 + 0.13I + 0.053T_{on} + 0.053S - 0.030DC + 0.026I^2 \quad (5)$$

$$\boldsymbol{R_a = 4.27 + 0.55I + 0.23T_{on} - 0.27S + 0.62DC} \quad (6)$$

Table 4. ANOVA and Response-table for MRR with Cr powder mixed dielectric fluid

Source	Sum-of-Squares	D-f	Mean-Square	F-Value	p-Value, Prob. > F	
Model	0.67	5	0.13	300.63	< 0.0001	S_t
I	0.46	1	0.46	1036.34	< 0.0001	S_t
T_{on}	0.080	1	0.080	179.32	< 0.0001	S_t
S	0.080	1	0.080	178.80	< 0.0001	S_t
DC	0.025	1	0.025	55.92	< 0.0001	S_t
I^2	0.024	1	0.024	52.80	< 0.0001	S_t
Residual	0.011	25	4.464E-004			
Lack of Fit	4.196E-003	19	2.209E-004	0.19	0.9976	NS
Pure Error	6.963E-003	6	1.160E-003			
Cor. Total	0.68	30				
Std. Dev.	0.021		R-Squared		0.9836	
Mean	0.48		Adj. R-Squared		0.9804	
C.V. %	4.43		Pred. R-Squared		0.9780	
PRESS	0.015		Adeq. Precision		69.832	

Table 5. ANOVA and Response-table for R_a with Cr powder mixed dielectric fluid

Source	Sum-of-Squares	D-f	Mean-Square	F-Value	p-Value, Prob. > F	
Model	18.87	5	3.77	203.27	< 0.0001	S_t
I	6.93	1	6.93	373.41	< 0.0001	S_t
T_{on}	1.30	1	1.30	69.87	< 0.0001	S_t
S	1.66	1	1.66	89.63	< 0.0001	S_t
DC	8.81	1	8.81	474.39	< 0.0001	S_t
T_{on}^2	0.17	1	0.17	9.08	0.0058	S_t
Residual	0.46	25	0.019			
Lack of Fit	0.43	19	0.022	3.52	0.0625	NS
Pure Error	0.038	6	6.362E-003			
Cor. Total	19.34	30				
Std. Dev.	0.14			R-Squared		0.9760
Mean	4.16			Adj. R-Squared		0.9712
C.V. %	3.28			Pred. R-Squared		0.9610
PRESS	0.75			Adeq. Precision		54.685

Table 6. C-C-R-D experimental-plan and process-responses without Cr powder mixed dielectric fluid

Exp. Number	Current (I) ampere	Pulse on-time (T_{on}) µs	Wheel Speed (S) RPM	Duty Cycle (DC)	MRR (mm^3/min) Experimental	MRR (mm^3/min) Predicted	R_a (µm) Experimental	R_a (µm) Predicted
1	-1	-1	-1	-1	0.255	0.240	3.37	3.14
2	1	-1	-1	-1	0.485	0.500	4.26	4.24
3	-1	1	-1	-1	0.338	0.346	3.52	3.60
4	1	1	-1	-1	0.586	0.606	4.70	4.70
5	-1	-1	1	-1	0.336	0.346	2.70	2.60
6	1	-1	1	-1	0.588	0.606	3.579	3.70
7	-1	1	1	-1	0.451	0.452	3.18	3.06
8	1	1	1	-1	0.701	0.712	4.23	4.16
9	-1	-1	-1	1	0.180	0.180	4.54	4.38
10	1	-1	-1	1	0.424	0.440	5.70	5.48
11	-1	1	-1	1	0.278	0.296	4.88	4.84

12	1	1	-1	1	0.538	0.546	6.23	5.94
13	-1	-1	1	1	0.293	0.286	3.879	3.84
14	1	-1	1	1	0.546	0.546	4.95	4.94
15	-1	1	1	1	0.382	0.392	4.49	4.30
16	1	1	1	1	0.650	0.652	5.59	5.40
17	-2	0	0	0	0.264	0.264	3.00	3.10
18	2	0	0	0	0.784	0.784	5.36	5.37
19	0	-2	0	0	0.329	0.314	3.50	3.81
20	0	2	0	0	0.552	0.526	4.45	4.73
21	0	0	-2	0	0.295	0.314	4.97	4.81
22	0	0	2	0	0.495	0.526	3.947	3.73
23	0	0	0	-2	0.485	0.480	3.36	3.03
24	0	0	0	2	0.355	0.360	5.45	5.51
25	0	0	0	0	0.417	0.420	4.28	4.27
26	0	0	0	0	0.467	0.420	4.29	4.27
27	0	0	0	0	0.398	0.420	4.36	4.27
28	0	0	0	0	0.415	0.420	4.25	4.27
29	0	0	0	0	0.422	0.420	4.18	4.27
30	0	0	0	0	0.436	0.420	4.169	4.27
31	0	0	0	0	0.369	0.420	4.39	4.27

Table 7. ANOVA and Response-table for MRR without Cr powder mixed dielectric fluid

Source	Sum-of-Squares	D-f	Mean-Square	F-Value	p-Value, Prob. > F	
Model	0.56	14	0.040	99.72	< 0.0001	S_t
I	0.39	1	0.39	958.87	< 0.0001	S_t
T_{on}	0.066	1	0.066	164.96	< 0.0001	S_t
S	0.066	1	0.066	164.96	< 0.0001	S_t
DC	0.021	1	0.021	51.98	< 0.0001	S_t
I^2	0.019	1	0.019	46.75	< 0.0001	S_t
Residual	6.447E-003	16	4.029E-004			
Lack of Fit	8.951E-004	10	8.951E-005	0.097	0.9992	NS
Pure Error	5.551E-003	6	9.252E-004			
Cor. Total	0.57	30				
Std. Dev.	0.020		R-Squared		0.9887	
Mean	0.44		Adj. R-Squared		0.9788	
C.V. %	4.60		Pred. R-Squared		0.9777	
PRESS	0.013		Adeq. Precision		42.420	

Table 8. ANOVA and Response-table for R_a without Cr powder mixed dielectric fluid

Source	Sum-of-Squares	d-f	Mean-Square	F-Value	p-Value, Prob. > F	
Model	20.40	14	1.46	93.35	< 0.0001	S_t
I	7.48	1	7.48	479.32	< 0.0001	S_t
T_{on}	1.37	1	1.37	88.01	< 0.0001	S_t
S	1.84	1	1.84	117.98	< 0.0001	S_t
DC	9.25	1	9.25	592.63	< 0.0001	S_t
T_{on}^2	0.092	1	0.092	5.92	0.0271	NS
Residual	0.25	16	0.016			
Lack of Fit	0.21	10	0.021	3.00	0.0955	NS
Pure Error	0.042	6	6.930E-003			
Cor. Total	20.65	30				
Std. Dev.	0.12		R-Squared		0.9879	
Mean	4.31		Adj. R-Squared		0.9773	
C.V. %	2.90		Pred. R-Squared		0.9392	
PRESS	1.26		Adeq. Precision		39.017	

Table 8. ANOVA and Response-table for R_a without Cr powder mixed dielectric fluid

Source	Sum-of-Squares	d-f	Mean-Square	F-Value	p-Value, Prob. > F	
Model	20.40	14	1.46	93.35	< 0.0001	S_t
I	7.48	1	7.48	479.32	< 0.0001	S_t
T_{on}	1.37	1	1.37	88.01	< 0.0001	S_t
S	1.84	1	1.84	117.98	< 0.0001	S_t
DC	9.25	1	9.25	592.63	< 0.0001	S_t
T_{on}^2	0.092	1	0.092	5.92	0.0271	NS
Residual	0.25	16	0.016			
Lack of Fit	0.21	10	0.021	3.00	0.0955	NS
Pure Error	0.042	6	6.930E-003			
Cor. Total	20.65	30				
Std. Dev.	0.12		R-Squared		0.9879	
Mean	4.31		Adj. R-Squared		0.9773	
C.V. %	2.90		Pred. R-Squared		0.9392	
PRESS	1.26		Adeq. Precision		39.017	

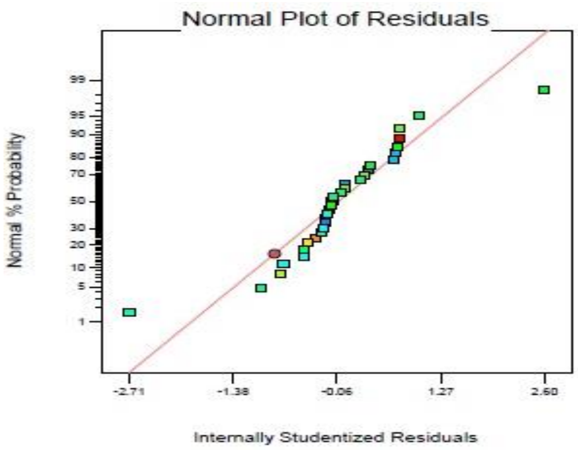

Fig. 3. N % probability plot of residual for MRR ……………… with Cr powder.

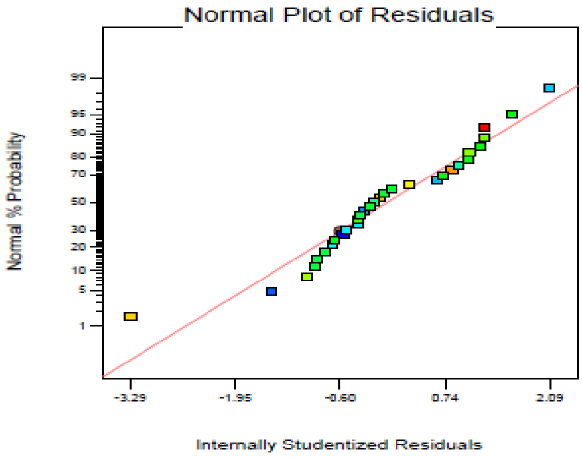

Fig. 4. N % probability plot of residual for R_a with Cr powder.

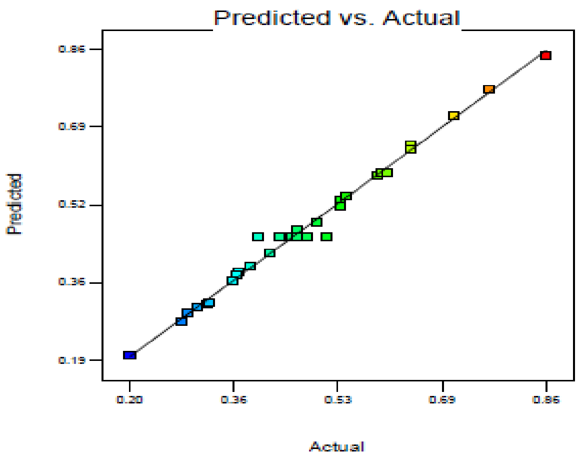

Fig. 5. Plot of actual and predicted output for MRR with Cr powder.

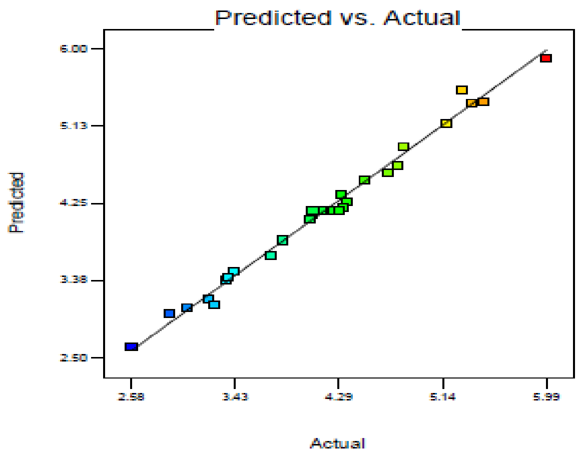

Fig. 6. Plot of actual and predicted output for R_a with Cr powder.

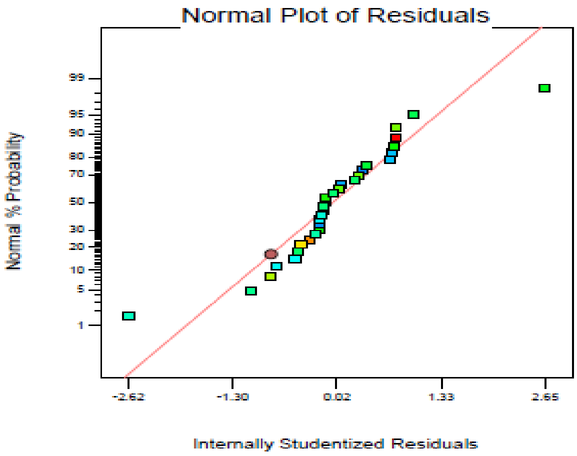

Fig. 7. N % probability plot of residual for MRR without Cr powder

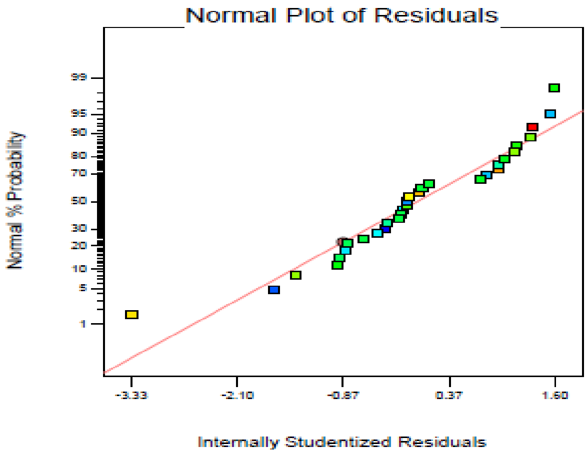

Fig. 8. N % probability plot of residual for R_a without Cr powder.

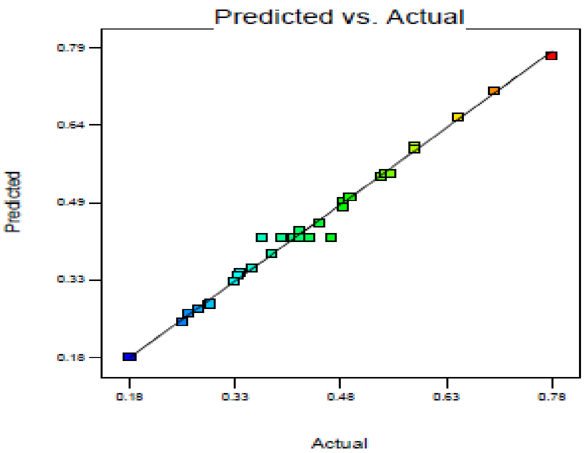

Fig. 9. Plot of actual and predicted output for output MRR without Cr powder.

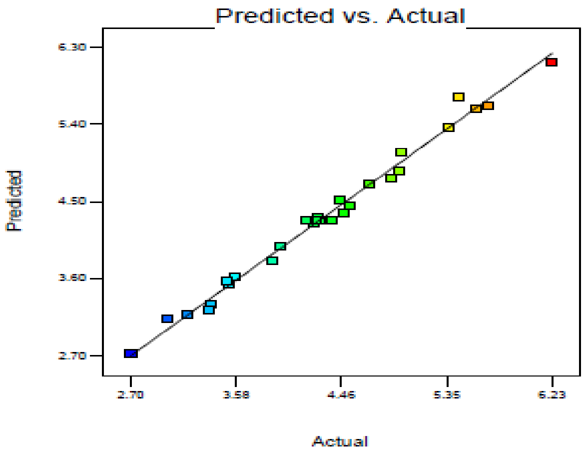

Fig. 10. Plot of actual and predicted for R_a without Cr powder.

The distinctive charts were plotted to foresee the conduct of input process factors over the process-responses using the “Eqs. (5) and (6)”.

5.1 ANOVA analysis for MRR and Ra model

The ANOVA outcomes for the MRR and R_a are depicted in the Tables 7 and 8 respectively. The N % probability graphs of residuals for MRR and R_a are displayed by the “Figs. 7 and 8” respectively. In addition, the predicted values obtained through the developed model were observed to be a cognate with the actual experimental values for MRR and R_a as depicted in “Figs. 9 and 10” respectively. The F-value of MRR and R_a model with absence of chromium powder blended DF is 99.72 and 93.35 respectively with value of $p < 0.0001$ for both the models so that these developed empirical equations of MRR and R_a are also able to express the relation among the input machining factors and the responses. The R-squared values of MRR and R_a model without chromium powder blended DF is 0.9887 and 0.9879 respectively indicates that the developed model are significant in describing the variation of MRR and R_a up-to 98.87 % and 98.79 %. There is negligible difference between Adj R-Squared and Pred R-Squared value for both the models. The values of CV are 4.60 and 2.90 for MRR and R_a model respectively. As CV becomes smaller in value, it will indicate towards improved precision and consistency of conducted experiments. The Adeq-Precision value for both the models is basically higher than the needed one and henceforth demonstrates a sufficient signal for both the models.

6 Analysis and interpretations of outcomes (from empirical models of MRR and R_a with chromium and absence of chromium powder in dielectric)

The investigation and interpretation of results are outlined here in Table 9 (refer the “Figs. 11 to 18”). It is seen that the best outcomes are acquired in S-EDDG machining-process with chromium powder in DF. This is the reason; the optimum combination of process parameters in this process is calculated with Cr powder mixed condition.

***Difference in MRR and R_a in PMS-EDDG process with chromium and absence of Cr Powder blended DF (refer Table 9)**

In the graphs from 11 to 14, the noticeable rise in MRR is seen in S-EDDG of Inconel 600 with chromium powder blended DF, as compared to the absence of powder in DF. The additional MRR is a direct result of the occurrence of series-discharge (along with spark-discharge and grinding operation taken place among the bronze-wheel and Inconel 600 surface in S-EDDG machining-process without chromium powder blended DF) in the EG because of the presence of Cr powder in dielectric-fluid and consequently formed the chain-like structure of powder particles in the IEG. This chain-like structure of powder particles is responsible for bridging the space among the electrodes and finally, series discharge occurred in IEG.

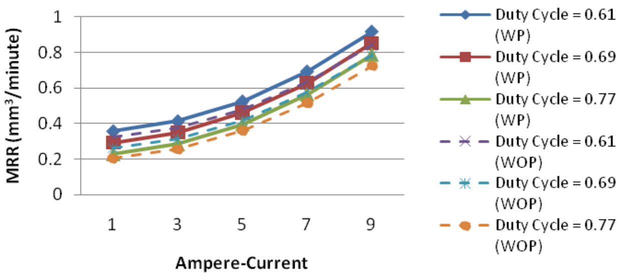

Fig. 11. Impact of ampere-current on MRR for various DC (WS = 600 rpm, T_{on}= 150μs)

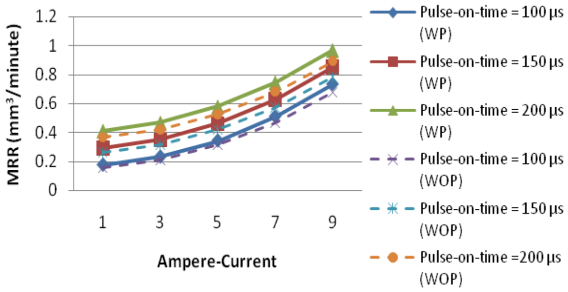

Fig. 12. Impact of ampere-current on MRR for various T_{on} (WS = 600 rpm, DC = 0.690)

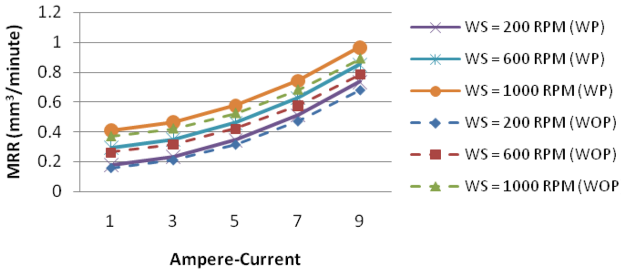

Fig. 13. Impact of ampere-current on MRR for various WS (T_{on}= 150μs, DC = 0.690)

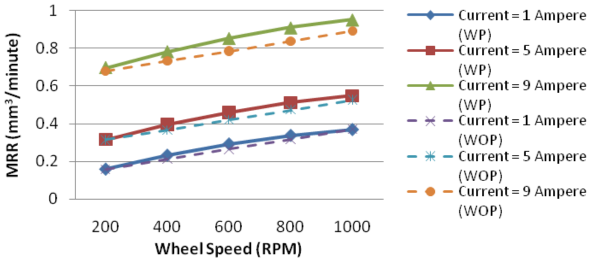

Fig. 14. Impact of WS on MRR for various ampere-current (T_{on}= 150μs, DC = 0.690)

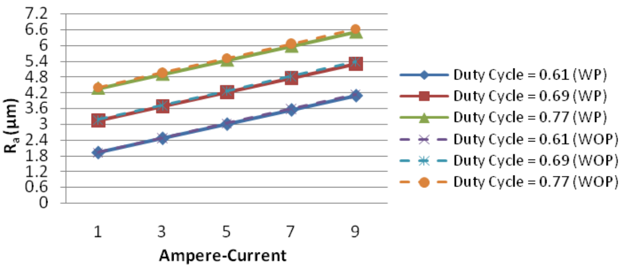

Fig. 15 Impact of ampere-current on R_a for various DC (WS = 600 rpm, T_{on}= 150μs).

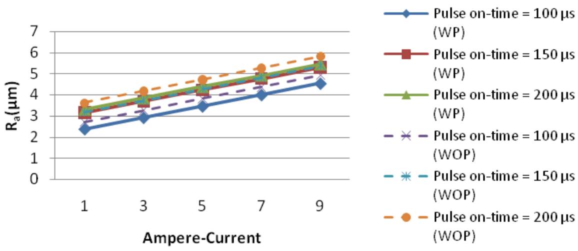

16. Impact of ampere-current on R_a for various T_{on} (WS = 600 rpm, DC = 0.690).

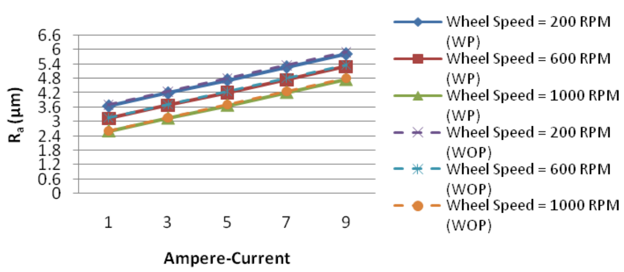

Fig. 17. Impact of ampere-current on R_a for various WS (T_{on}= 150μs, DC = 0.690)

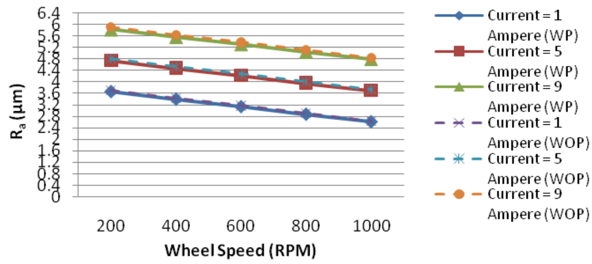

Fig. 18. Impact of WS on R_a for various ampere-current (T_{on} = 150μs, DC = 0.690)

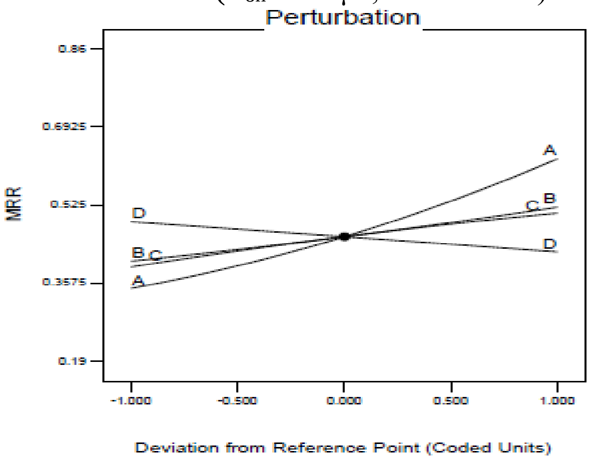

Fig. 19. Perturbation plots for MRR with Cr powder

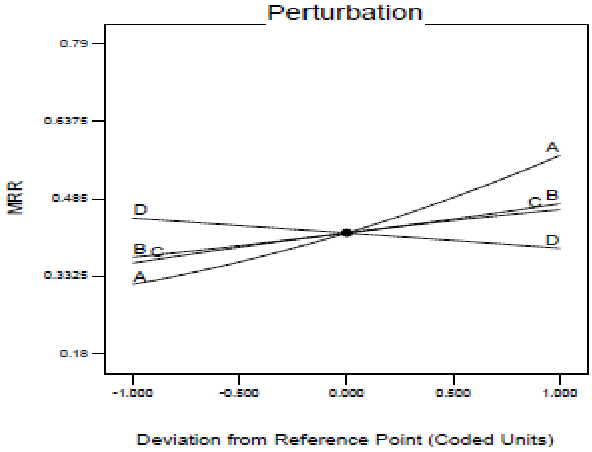

Fig. 20. Perturbation plots for MRR without Cr powder

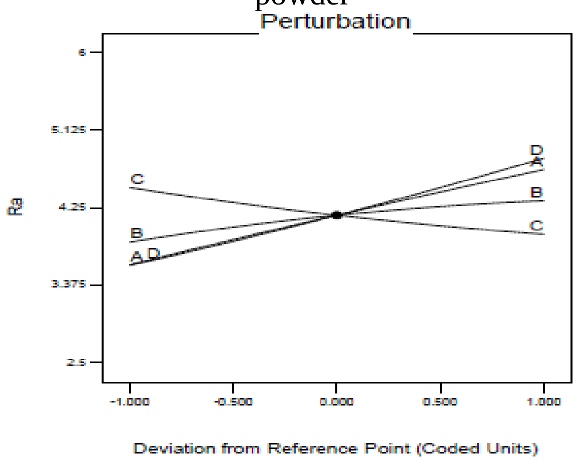

Fig. 21. Perturbation plots for R_a with Cr powder.

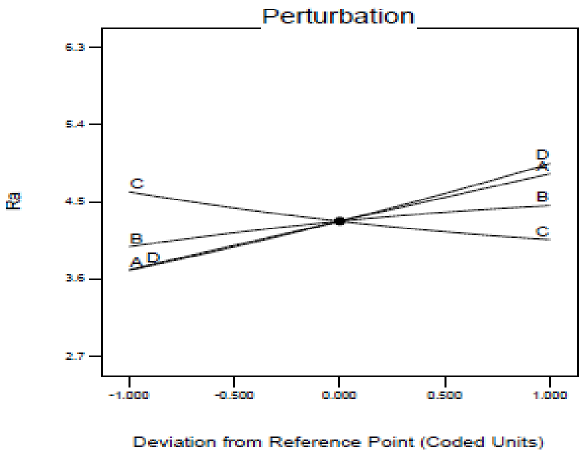

Fig. 22. Perturbation plots for R_a without Cr powder

Whereas, with reference to "Figs. from 15 to 18", the noticeable rise in surface finish is observed in S-EDDG of Inconel 600 with chromium power blended DF, as compared to the absence of Cr powder in DF. It occurred on account of the presence of Cr powder in the electrode gap reformed the plasma channel. The plasma channel is wider and larger and the discharge spark-energy is uniformly dispersed among the Cr powder particles and consequently responsible for the development of narrower size cavities on the worked surface.

The perturbation plot for MRR with and without Cr powder mixed condition is displayed in "Figs. 19 and 20" respectively. The sharp-incline for current (A) and DC (D) demonstrates towards high affectability of MRR towards them. Similarly, lines of less steep for WS (C), and T_{on} (B) show less affectability of MRR towards them. The MRR is more with chromium powder as compared to without Cr powder blended DF.

The perturbation plot for R_a with and without Cr powder mixed condition is displayed in "Figs. 21 and 22" respectively. The sharp-incline for current (A) and WS (C) demonstrates towards high affectability of R_a towards them. Similarly, lines of less steep for DC (D), and T_{on} (B) show less affectability of R_a towards them. The R_a is less with Cr powder as compared to without Cr powder blended DF.

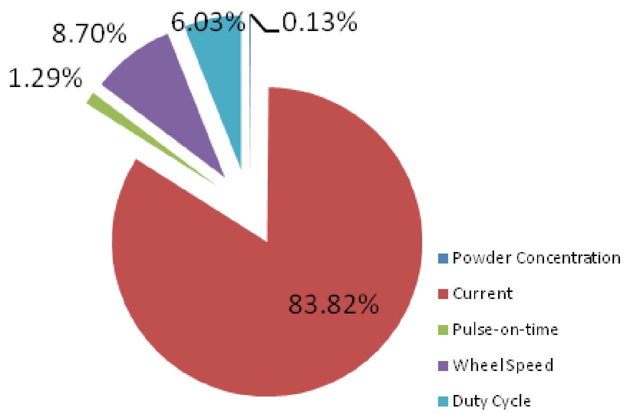

Fig. 23. % contribution of machining process - factors on WMPI.

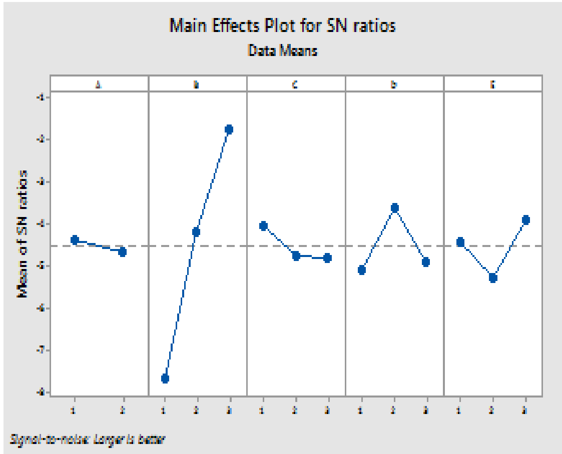

Fig. 24. S/N-ratio plot of WMPI

Table 9 Analysis of outcomes and interpretation of Figs 11 to 18

Figure No.	**Continual-line/ Dot-line**	**Experimental Condition (with Cr and absence of Cr powder)**	**Tendency 1 in Figure**	**Cause for Tendency 1 in Figure**	**Tendency 2 in Figure**	**Cause for Tendency 2 in Figure**
11	Continual-line	Presence of Cr powder	MRR enhances with the growth in ampere current.	The additional spark discharge is produced due to the growth in ampere current.	MRR enhances with the decrease in duty cycle.	Pulse off time is improving persistently to get the descending pattern in the duty-cycle. This is why adequate flushing and deionization time is accessible for the dielectric.
	Dot line	Absence of Cr powder				
12	Continual-line	Presence of Cr powder	,,	,,	MRR enhances with the growth in pulse-on-time.	Pulse-on-time is growing-up continuously. This is why sufficient time is available for the heat-conduction.
	Dot line	Absence of Cr powder				
13	Continual-line	Presence of Cr powder	,,	,,	MRR enhances with the rise in wheel speed.	Additional discharge energy is dissipated due to the increase in wheel speed. It occurs due to the current-flow rate in the grinding area rises.
	Dot line	Absence of Cr powder				
14	Continual-line	Presence of Cr powder	MRR upgrades	Flushing enhances and	MRR enhances	The additional spark discharge is produced

	Dot line	Absence of Cr powder	with the hike in wheel-speed.	width of gap decreases due to the increase in wheel speed.	with the growth in ampere current.	due to the growth in ampere current.
15	Continual-line	Presence of Cr powder	R_a enhances with the growth in ampere current.	The additional spark discharge is produced due to the growth in ampere current. Hence, bigger size cavities are produced on the work surface.	R_a enhances with the rise in duty cycle.	Pulse-off-time is reducing consistently to bring the increasing tendency in the DC. This is why; lesser deionization and flushing time is available for the dielectric.
	Dot line	Absence of Cr powder				
16	Continual-line	Presence of Cr powder	”	”	R_a enhances with the growth in pulse-on-time.	T_{on} is growing consistently. So that additional time is accessible for the warmth conduction in w/p. The MRR enhances due to the thermal-softening of w/p and subsequently, Ra enhances because of the production of bigger-size cavities.
	Dot line	Absence of Cr powder				
17	Continual-line	Presence of Cr powder	”	”	R_a reduces with the growth in WS.	All molten eroded work piece materials from IEG are swept aside by the efficient flushing. This is attained by enhancing in WS. The adherence of worn out unflushed molten substances on surface of work is lowered.
	Dot line	Absence of Cr powder				
18	Continual-line	Presence of Cr powder	R_a reduces with growth in wheel speed.	Flushing enhances with growth in WS and reduces the R_a.	R_a enhances with the growth in ampere current.	The additional spark discharge is produced because of the growth in ampere current. Hence, bigger size pits are produced on the worked surface.
	Dot line	Absence of Cr powder				

7 Parametric Optimization with Grey-TM based WPCA approach

One set of 18 experiments was performed in accordance with L_{18} O-A on Cr Powder Mixed S-EDDG frame-up with Inconel 600 material. Dependent upon beginning test outcomes and EDM machine confine, the level of process factors was picked as portrayed in Table 10. The proposed methodology for multi response optimization of process factors is described as follows.

The collected values of experimental responses were normalized using the “Eqs. (7), and (8)”, to limit the redundancies as well as to limit the dependency among the output-responses.

The MRR has the higher the better execution a quality is normalized using "Eq. (7)" while the R_a has the lower is the better execution attributes is normalized using the "Eq. 8". Table 11 depicts the L_{18} O-A, process-responses, log-S, and normalised log-S value.

$$x_i^*(t) = \frac{x_i^{(o)}(t) - m\,in.\,x_i^{(o)}(t)}{m\,ax.\,x_i^{(o)}(t) - m\,in.\,x_i^{(o)}(t)} \tag{7}$$

$$x_i^*(t) = \frac{max.\,x_i^{(o)}(t) - x_i^{(o)}(t)}{max.\,x_i^{(o)}(t) - min.\,x_i^{(o)}(t)} \tag{8}$$

Where, $x_i^{(o)}(t)$= Original-arrangement, $x_i^{(*)}(t)$= Normalized Value, $min.\,x_i^{(o)}(t)$= Minimal estimation of $x_i^{(o)}(t)$, $max.\,x_i^{(o)}(t)$ = Extreme estimation of$x_i^{(o)}(t)$, i =1, 2, 3, . . p; t =1, 2. . . q; p = Entire experiment, and q = Full observation data.

The deviation sequence [$\Delta_{oi}(t)$] and GR coefficient is determined using the "Eqs. (9), and (10)" respectively. The deviation sequence gives the variation and GR coefficient provides the relational degree among the compatibility and reference sequence.

$$\Delta_{oi}(t) = \left| x_o^{(*)}(t) - x_i^*(t) \right| \tag{9}$$

$$\gamma\left(x_o^{(*)}(t), x_i^{(*)}(t)\right) = \frac{\Delta_{min.} + \zeta\Delta_{max.}}{\Delta_{oi}(t) + \zeta\Delta_{max.}} \tag{10}$$

$$0 < \gamma\left(x_0^*(t), x_i^*(t)\right) \leq 1, \Delta_{\max.} = \max_{\forall j \in i}.\ \max_{\forall t}.\left|x_o^*(t) - x_j^*(t)\right|, \Delta_{\min.} = \min_{\forall j \in i}.\ \min_{\forall t}.\left|x_o^*(t) - x_j^*(t)\right|$$

Here,

$x_o^{(*)}(t)$	Reference-Sequence;	$\zeta =$	Distinguishing-Coefficient, $\zeta \in [0,1]$
$x_i^*(t)$	Comparability-Sequence.		

In PCA technique, the PC_1 portrays the maximal change in the gathered data and the PC_2 depicts the rest of the difference that was left by the PC_1 etcetera. Principal components are evaluated using the "Eqs. (11) to (13)".. PC analysis is utilized to clarify the structure of covariance-variance by the linear coalition of the primal factors. Expect that there are p-parts to speak to the framework inconstancy. By utilizing PC Analysis, the framework changeability might be clarified by a less number, m (m ≤ p), of the PCs, i.e. m PCs will represent the larger part of difference inside the primal p factors. For the response-factors, Z_1, Z_2 …, Zp, there is the accompanying PCs i.e. *Yi* (*i*= 1, 2, 3…, m). These PCs can be expressed by the following "Eqs. (11) to (13)".

$$Y_1 = a_{11}Z_1 + a_{12}Z_2 + \ldots.. + a_{ip}Z_P \tag{11}$$

$$Y_2 = a_{21}Z_1 + a_{22}Z_2 + \ldots.. + a_{2p}Z_P \tag{12}$$

$$Y_m = a_{m_1}Z_1 + a_{m_2}Z_2 + \ldots.. + a_{m_p}Z_P \tag{13}$$

where

$$a_{m1}^2 + a_{m2}^2 + \cdots + a_{mp}^2 = 1.$$

Table 10. Input factors and its range

Symbol	Control Processes Parameters	Level-1	Level-2	Level-3
PC	Cr Powder Concentration (gm/litre)	1.5	3	-
I	Current (Ampere)	1	3	5
T_{on}	Pulse-on-time (μs)	50	100	150
S	Wheel Speed (RPM)	300	500	700
DC	Duty Cycle	0.57	0.60	0.63

Table 11. L_{18} O-A, process-responses, log-S, and normalised log-S value

Exp.	Control Factors					Responses		Log-S value		Normalised Log-S value	
No.	PC	I	T_{on}	S	DC	MRR	R_a	MRR	R_a	MRR	R_a
1	1	1	1	1	1	0.198	1.390	-14.0667	-2.8603	0.455	0.199
2	1	1	2	2	2	0.210	1.200	-13.5556	-1.5836	0.539	0.125
3	1	1	3	3	3	0.199	0.911	-14.0229	0.8096	0.462	-0.014
4	1	2	1	1	2	0.217	3.010	-13.2708	-9.5713	0.586	0.590
5	1	2	2	2	3	0.240	4.154	-12.3958	-12.3693	0.730	0.752
6	1	2	3	3	1	0.202	3.170	-13.8930	-10.0212	0.483	0.616
7	1	3	1	2	1	0.290	4.920	-10.7520	-13.8393	1.000	0.838
8	1	3	2	3	2	0.215	4.830	-13.3512	-13.6789	0.573	0.829
9	1	3	3	1	3	0.228	6.240	-12.8413	-15.9037	0.656	0.958
10	2	1	1	3	3	0.207	1.250	-13.6806	-1.9382	0.518	0.146
11	2	1	2	1	1	0.144	0.937	-16.8328	0.5652	0.000	0.000
12	2	1	3	2	2	0.159	1.250	-15.9721	-1.9382	0.142	0.146
13	2	2	1	2	3	0.240	5.230	-12.3958	-14.3700	0.730	0.869
14	2	2	2	3	1	0.196	3.630	-14.1549	-11.1981	0.440	0.684
15	2	2	3	1	2	0.187	2.070	-14.5632	-6.3194	0.373	0.400
16	2	3	1	3	2	0.206	5.110	-13.7227	-14.1684	0.511	0.857
17	2	3	2	1	3	0.183	5.880	-14.7510	-15.3875	0.342	0.928
18	2	3	3	2	1	0.242	6.780	-12.3237	-16.6246	0.742	1.000

Y_1 is known as the first important PC, Y_2 is known as the second key PC and a_{m1}, a_{m2}…, a_{mp} are the components of the eigen-vector comparing to the m^{th} biggest eigen-value. The m^{th} segment-coefficient is the parts of the eigen-vector matching to the m^{th} greatest eigen-values. Nonetheless, there are as yet two evident inadequacies in the PCA technique. To start with, when in excess of one key segment (i.e. PC) is chosen whose eigen-value is more prominent than 1, the required exchange-off for a practical result is obscure; and second, the MPI can't supplant the multi-response result when the picked PC can only be clarified by aggregate-variation. WPCA technique is utilized here to defeat the inadequacies of multi-response issue in the PCA approach. The WPCA technique utilizes the clarified variation as the weight to join all PCs with the end goal to frame a WMPI. WPCA is a viable method to depict the slight number of segments which is accountable for the main sources of variance in a set-arrangement of related quality-properties. WPCA has been conducted on GRC of every quality-characteristic and determine the Eigen-value, and Eigen-vector from concurrence matrix created by GRC. Minitab software is used for WPC analysis. The WMP index can be utilized to decide the optimal setting of process parameters. The greater the estimation of WMPI suggests the better the product-quality. WMPI is computed utilizing the “Eq. (14)”.

$$WMPI = \sum_{i=1}^{m} W_m \, PC_m \qquad (14)$$

where, W_m is the weight of i^{th} PC’s. Table 12 showed the deviation-sequence, GRC, WMPI, Log-S value of WMPI. The eigen-values and eigen-vector is displayed in Table 13.

Table 12. Deviation-sequence, GRC, WMPI, and Log-S value of WMPI

Exp. No.	Deviation Sequence		GRC		WMPI	Log-S value of WMPI
	MRR	R_a	MRR	R_a		
1	0.545	0.801	0.478	0.384	0.444	-7.060
2	0.461	0.875	0.520	0.364	0.444	-7.053
3	0.538	1.014	0.482	0.330	0.406	-7.819
4	0.414	0.410	0.547	0.549	0.585	-4.661
5	0.270	0.248	0.649	0.669	0.706	-3.024
6	0.517	0.384	0.492	0.566	0.576	-4.784
7	0.000	0.162	1.000	0.755	0.893	-0.982
8	0.427	0.171	0.539	0.745	0.720	-2.851
9	0.344	0.042	0.593	0.923	0.865	-1.258
10	0.482	0.854	0.509	0.369	0.444	-7.053
11	1.000	1.000	0.333	0.333	0.355	-8.986
12	0.858	0.854	0.368	0.369	0.393	-8.108
13	0.270	0.131	0.649	0.792	0.793	-2.012
14	0.560	0.316	0.472	0.613	0.603	-4.396
15	0.627	0.600	0.444	0.455	0.481	-6.359
16	0.489	0.143	0.506	0.778	0.732	-2.716
17	0.658	0.072	0.432	0.874	0.773	-2.235
18	0.258	0.000	0.659	1.000	0.944	-0.503

Table 13. Eigen-values and Eigen-vector

	PC_1	PC_2
Eigen value	1.5070	0.4930
Eigen vector	[0.707, 0.707]	[-0.707, 0.707]
Proportion	0.754	0.246
Cumulative	0.754	1.0

Table 14. Response and ANOVA-table for WMPI.

Response-table				Symbol	ANOVA-table					
Level-1	Level-2	Level-3	Max-Min		DF	SS	MS	F	P	C (%)
-4.388^p	-4.708		0.319	PC	1	0.000824	0.000824	0.49	0.506	0.13
-7.680	-4.206	-1.758^p	5.922	I	2	0.496380	0.248190	146.37	0.000	83.82
-4.081^p	-4.758	-4.805	0.725	T_{ON}	2	0.007650	0.003825	2.26	0.167	1.29
-5.093	-3.614^p	-4.937	1.479	S	2	0.051567	0.025784	15.21	0.002	8.70
-4.452	-5.291	-3.900^p	1.391	DC	2	0.035740	0.017870	10.54	0.006	6.03
				Error	8	0.013565	0.001696			
				Total	17	0.605727				

8 Discussion

ANOVA examination was conducted on WMPI. The result of ANOVA and the impact of several machining factors on the WMPI are listed in Table 14. The % contribution of machining factors is depicted in "Fig. 23". "Fig. 24" delineated the S/N-ratio plot of WMPI. The optimal setting of several machining factors determined through GRA-TM based WPCA approach in Cr powder mixed S-EDDG of Inconel 600, is PC at first level, I at third level, T_{on} at first level, S at second level, and DC at third level. The current, wheel speed, and duty cycle are the most significant factors that influence process performance characteristic.

8.1 Confirmation test

The estimated $\hat{\alpha}$ grade is computed utilizing the "Eq. (15)".

$$\hat{\alpha} = \alpha_m + \sum_{i=1}^{n} \left(\bar{\alpha}_i - \alpha_m\right) \tag{15}$$

Where, α_m= average grade, $\bar{\alpha}_i$ = optimal average grade, and 'n' is the total main-process factors which influence the multi-output performance characteristics. To assure the improvement in quality-performance, an affirmation test is carried out. The result of this test is shown in Table 15.

Table 15. Result of confirmation test

Factor-Level	Initial Process-Parameters	Optimal Process-parameter	
		Prediction	Experiment
	$PC_1 I_1 T_{on_1} S_1 D_1$	$PC_1 I_3 T_{on_1} S_2 D_3$	$PC_1 I_3 T_{on_1} S_2 D_3$
MRR (mm^3/min)	0.198	-	0.276
R_a (μm)	1.390	-	5.010
WMPI	0.444	0.97	0.858
Improvement in WMPI is 0.414			

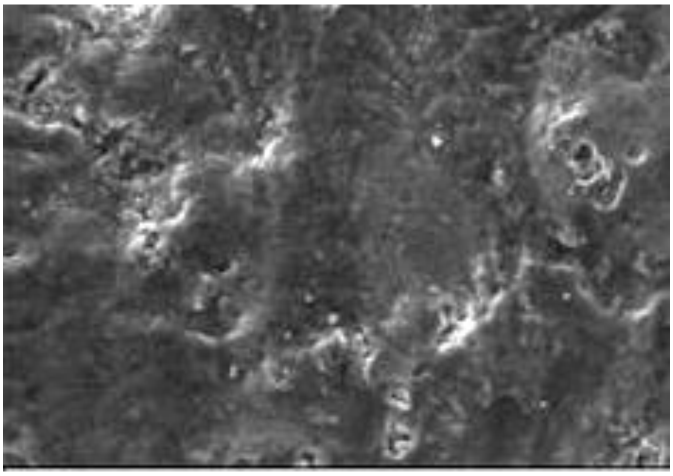

a)

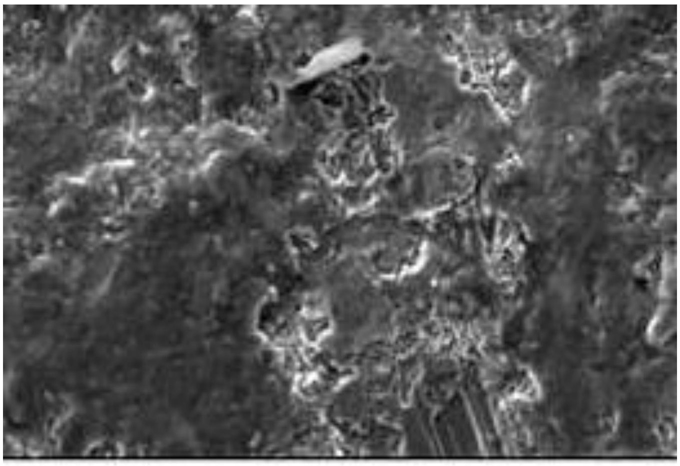

b)

Fig. 25. Effect of presence of chromium and absence of chromium powder in dielectric fluid on the surface generation of machined surfaces of Inconel 600 through S-EDDG process at optimum condition a) S-EDDG produced surface with Cr powder mixed dielectric fluid, b) S-EDDG produced surface without powder mixed dielectric fluid *(I = 5 A, T_{on} = 50 μs, DC = 0.63 and WS = 500 RPM)*

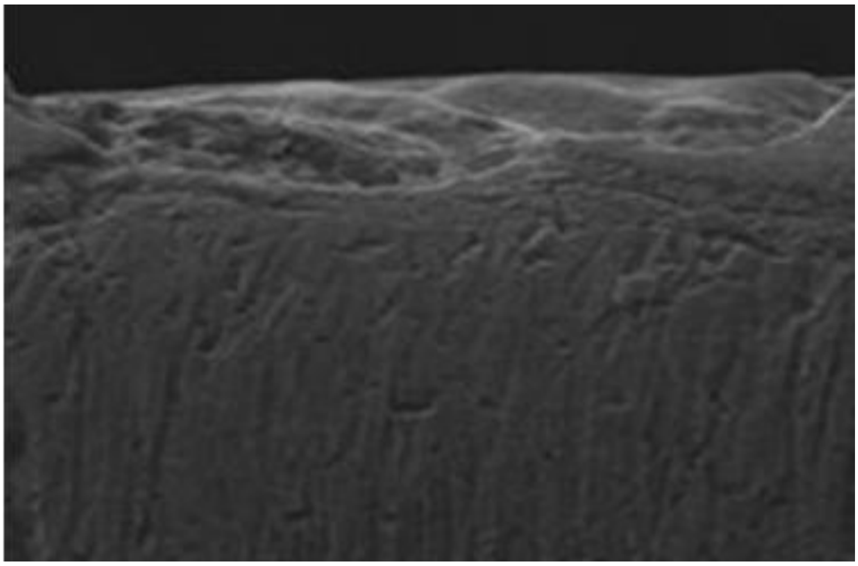

a)

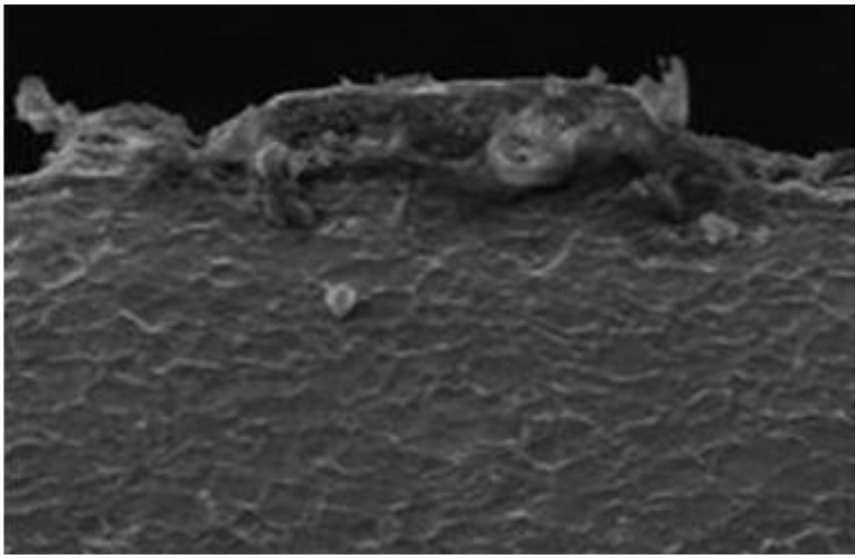

b)

Fig. 26. Effect of presence of chromium and absence of chromium powder in dielectric fluid on the WRLT of machined surface of Inconel 600 through S-EDDG process at optimum condition a) With Cr powder mixed dielectric fluid; t = 47 μm; b) Without Cr powder mixed dielectric fluid; t = 32 μm; *(I = 5 A, T_{on} = 50 μs, DC = 0.63 and WS = 500 RPM)*

9 Analysis of surface generation and WRLT in S-EDDG of Inconel 600 with chromium and absence of Cr powder blended DF at optimum condition

The SEM investigation has been conducted on the S-EDDG produced surfaces with chromium and absence of Cr powder blended DF at the optimum condition. In the "Figs. 25 (a) and (b)", it was seen that the detectable ascent in the surface-finish of work-material with Cr powder as compared to the absence of Cr powder blended in DF. The presence of Cr powder in between the electrodes reformed the plasma channel. The produced spark energy is evenly shared among the Cr powder particles and thus accountable for the creation of narrower size pits on the worked surface.

If the melted material from surface isn't flushed rapidly, it will re-set on account of the cooling impact of the DF and stick to the created machined-surface. This stuck layer is known as the recast-white-layer. In the "Fig. 26 (a) and (b)", it is seen that wrl thickness is more with chromium as compared to absence of chromium powder blended DF. It is happened due to the presence of Cr powder particles in DF increase the gap spacing among the electrodes and consequently responsible for ineffective flushing condition in IEG as compared to the absence of Cr powder particles in DF.

CONCLUSIONS

The following conclusions could be drawn based on the examination of experimental results, understanding of "Figs. 3 to 22, 25, and 26", integrated optimization approach, and S-E-M pictures examinations:

1. MRR, surface-finish, and white recast layer thickness is more in chromium powder mixed dielectric fluid in contrast to dielectric fluid without it, during S-EDDG of Inconel 600.

2. The maximum MRR is attained when current, T_{on}, and wheel-speed are at top levels. In a similar way, the maximum MRR is attained when DC is at the minimal level.

3. The minimal R_a is attained when, current, T_{on}, DC are at the minimal levels. In a similar way, the maximum R_a is attained when WS is at the minimal level.

4. Surface craters on the machined surface are narrower and smaller due to presence of chromium powder in contrast to DF without it, during S-EDDG of Inconel 600.

5. It is seen through ANOVA outcomes that the percentage contribution of several process variables on the process performance characteristics is powder concentration (0.13 %); current (83.82 %); pulse on time (1.29 %); wheel speed (8.70 %); and duty cycle (6.03 %). The current, wheel speed, and duty cycle are the significant variables which influence the process performance.

6. The Weighted Multiple Performance Index has been enhanced by 0.414.

REFERENCES

[1] Aggarwal, V., Khangura, S. S., Garg, R. K. "Parametric modeling and optimization for wire electrical discharge machining of Inconel 718 using response surface methodology", International Journal of Advanced Manufacturing Technology 79 (1–4), pp. 31 – 47, **2015**. DOI: http: 10.1007/s00170-015-6797-8

[2] Shaw, M.C, Nakayama, K. "Machining high strength materials", CIRP Annal 15, pp. 45 – 59, **1967**. https://www.cirp.net/component/cirppubli/?task=searchpublic&year=1966

[3] Luo, Y. F. "The dependence of inter space discharge transitivity upon the gap debris in precision electro discharge machining", Journal of Materials Processing Technology 68, pp. 121 – 131, **1997**. DOI: 10.1016/S0924-0136(96)00019-2

[4] Ho, K. H., Newman, S. T. "State of the art electrical discharge machining (EDM)", International Journal of Machine Tools & Manufacture 43, pp. 1287 – 1300, **2003**. DOI: 10.1016/S0890-6955(03)00162-7

[5] Lee, H. T., Tai, T. Y. "Relationship between EDM parameters and surface crack formation", Journal of Materials Processing Technology 142, pp. 676 – 683, **2003**. DOI: 10.1016/S0924-0136(03)00688-5

[6] Kao, J. Y., Tsao, C. C., Wang, S. S., Hsu, C. Y. "Optimization of the EDM parameters on machining Ti–6Al–4V with multiple quality characteristics", International Journal of Advanced Manufacturing Technology 47, pp. 395 – 402, **2010**. DOI: 10.1007/s00170-009-2208-3.

[7] Tzeng, Y. F., Lee, C. Y. “Effects of Powder Characteristics on Electro discharge Machining Efficiency”, International Journal of Advanced Manufacturing Technology 17, pp. 586 – 592, **2001**. DOI: 10.1007/s001700170142

[8] George, P. M., Raghunath, B. K., Manocha, L. M., Warrier, A. M. “EDM machining of carbon–carbon composite - a Taguchi approach”, Journal of Materials Processing Technology 145, pp. 66 – 71, **2004**. DOI: 10.1016/S0924-0136(03)00863-X

[9] Modi, M., Jha, S. “Modelling and Analysis of Powder Mixed Electric Discharge Machining”, International Journal of Mechanical Engineering 2, pp. 219 – 223, **2009**.

[10] Singh, G. K., Yadava, V, Kumar, R. “Diamond Face Grinding of WC-Co Composite with Spark Assistance: Experimental Study and Parameter Optimization”, International Journal of Precision Engineering and Manufacturing 11 (4), pp. 509 – 518, **2010**. DOI: 10.1007/s12541-010-0059-3

[11] Gauri, S. K., Chakraborty, S. “A study on the performance of some multi-response optimisation methods for WEDM processes”, International Journal of Advanced Manufacturing Technology 49, pp. 155 – 166, **2010**. DOI: 10.1007/s00170-009-2391-2

[12] Lin, J. L., Lin, C. L. “The use of grey-fuzzy logic for the optimization of the manufacturing process”, Journal of Materials Processing Technology 160, pp. 9 – 14, **2005**. DOI: 10.1016/j.jmatprotec.2003.11.040

[13] Modi, M., Agarwal, G. “Powder-Mixed Electro-Discharge Diamond Surface Grinding Process: Modelling, Comparative Analysis and Multi-Output Optimization Using Weighted Principal Components Analysis”, SV-JME 59, pp. 735 – 747, **2013**. DOI: 10.5545/sv-jme.2013.1146

[14] Modi, M., Agarwal, G. “Optimization of Electro-Discharge Diamond Surface Grinding Process Parameters with Multiple Performance Characteristics of Ti-6Al-4V using Grey-Taguchi Approach”, Advanced Materials Research 622, pp. 14 – 18, **2013**. DOI: 10.4028/www.scientific.net/AMR.622-623.14

[15] Chen, S. L., Yan, B. H., Huang, F. Y. “Influence of kerosene and distilled water as dielectrics on the electric discharge machining characteristics of Ti–6A1–4V”,Journal of Materials Processing Technology 87, pp. 107 – 111, **1999**. DOI: 10.1016/S0924-0136(98)00340-9

[16] Liao, H. C. “Multi-response optimization using weighted principal component”, International Journal of Advanced Manufacturing Technology 27, pp.720 – 725, **2006**. DOI: 10.1007/s00170-004-2248-7

[17] Kumar, S., Singh, R., Batish, A., Singh T. P. “Modeling the tool wear rate in powder mixed electro-discharge machining of titanium alloys using dimensional analysis of cryogenically treated electrodes and workpiece”, Journal of Processing Mechanical Engineering, 231 (2), pp. 271 – 282, **2017**. DOI: 10.1177%2F0954408915593875

[18] Ramesh, S., Jenarthanan, M. P., Bhuvanesh Kanna, A. S. “Experimental investigation of powder-mixed electric discharge machining of AISI P20 steel using different powders and tool materials”, Multidiscipline Modeling in Materials and Structures 14 (11), **2017**. DOI: 10.1108/MMMS-04-2017-0025

[19] Modi, M., Agarwal, G. “Design, Development & Experimental Investigation of Electro-Discharge Diamond Surface Grinding of Ti-6Al-4V”, Advanced Materials Research 418, pp. 1478 – 1481, **2011**. DOI: 10.4028/www.scientific.net/AMR.418-420.1478

[20] Modi, M., Agarwal, G. “Influence of Dielectric Jet flushing during Electro Discharge Diamond Surface Grinding process”, Advanced Materials Research 652, pp. 2187 – 2190, **2013**. DOI: 10.4028/www.scientific.net/AMR.652-654.2187

[21] Kumar, S., Dhingra, A. K., kumar, S. “Parametric optimization of powder mixed electrical discharge machining for nickel based super alloy inconel-800 using response surface methodology”, Mechanics of Advanced Materials and Modern Processes, Vol. 3:7, 2017, DOI: https://doi.org/10.1186/s40759-017-0022-4

[22] Modi, M., Agarwal, G., Patil, V., Khare, A., Shukla, S., Shankhla, A. “Modeling and analysis of turning process on lathe machine By Taguchi and ANOVA approach”, International Journal of Scientific & Technology Research 8 (10), pp. 1466 – 1470, **2019**. http://www.ijstr.org/final-print/oct2019/Modeling-And-Analysis-Of-Turning-Process-On-Lathe-Machine-By-Taguchi-And-Anova-Approach.pdf

[23] Modi, M., Agarwal, G., Patil, V., Bhatia, U., Pancholi, R. “Parametric Optimization in Drilling of Al–SiC Composite Using Taguchi Method”, International Journal of Scientific & Technology Research 8 (9), pp. 2019 – 22, **2019**. http://www.ijstr.org/final-print/sep2019/Parametric-Optimization-In-Drilling-Of-Alsic-Composite-Using-Taguchi-Method.pdf

[24] Chander, P., Kansal, H.K., Pabla, B. S., Puri, S. “Experimental Investigations in Powder Mixed Electric Discharge Machining of Ti-35Nb-7Ta-5Zr β- Titanium Alloy”, Materials and Manufacturing Processes 32 (3), pp. 1 – 13, **2016**. DOI: 10.1080/10426914.2016.1198018

[25] Razak, M. A., Rani, A.M.A., Saad, N. M., Littlefair, G., Aliyu, A. A., “Controlling corrosion rate of Magnesium alloy using powder mixed electrical discharge machining”, IOP Conf. Series: Materials Science and Engineering 344, pp. 1 – 10, **2018**. DOI: 10.1088/1757-899X/344/1/012010

[26] Modi, M., Agarwal, G. “Effect of aluminium and chromium powder mixed dielectric fluid on electrical discharge machining effectiveness”, Advances in Production Engineering & Management Journal 14 (3), pp. 323 – 332, **2019**. DOI: 10.14743/apem2019.3.330

[27] Modi, M., Agarwal, G. “Integrated statistical methodology for optimizing the machining parameters in SIC powder mixed – EDDSG process to machine TI6AL4V”, Materiali in tehnologije / Materials and technology Journal 53 (3), pp. 357 – 366, **2019**. DOI: 10.17222/mit.2018.194

[28] De, D., Nandi, T., Bandyopadhyay, A. “Parametric study for wire cut electrical discharge machining of sintered titanium”, Strojnícky časopis – Journal of Mechanical Engineering 69 (1), pp. 17 – 38, **2019**. DOI: 10.2478/scjme-2019-0002

[29] Raturi, H. P., Prasad, L., Pokhriyal, M., Tirth, V. “An estimating the effect of process parameters on metal removal rate and surface roughness in WEDM of composite AL6063/SIC/AL_2O_3 by Taguchi Method”, Strojnícky časopis – Journal of Mechanical Engineering 67 (2), pp. 25 – 36, **2017**. DOI: 10.1515/scjme-2017-0015

[30] Yadav, S. U., Yadav, V. “Modelling and optimisation of process parameters of electrical discharge diamond drilling of nimonic alloy - an aerospace material”, International Journal of Industrial and Systems Engineering (IJISE) 29 (4), pp. 507 – 532, **2018**. DOI: 10.1504/IJISE.2018.094270

[31] Koing, W., Cronjager, L., Spur, G., Tonshoff, H. K., Vigneau, M., Zdeblick, W.J., "Machining of new materials", annals of CIRP 39 (2), pp. 673 – 681, **1990**. DOI: 10.1016/s0007-8506(07)63004-2

[32] Jain V. K. "Advanced Machining Processes", Allied Publishers Pvt. Ltd., New Delhi, India, **2002**.

[33] Design Expert Software, Version 8.0.7.1, User Guide, "Technical manual", Stat-Ease Inc., Minneapolis, MN, **2010**.

[34] Montgomery, D. C. "Design, and analysis of experiments", Wiley, New York, **2009**.

Abbreviations

ANOVA	Analysis of variance
S-EDDG	Electro Discharge Diamond Surface Grinding
EDDG	Electro Discharge Diamond Grinding
PMS-EDDG	Powder Mixed Surface Electro Discharge Diamond Grinding
DA	Dimensional Analysis
PMED-M	Powder Mixed ED-Machining
PCA	Principal Component Analysis
C-C-R-D	Central Composite Rotary Design
CV	Coefficient of Variation
PBED-M	Powder Blended ED-Machining
EDM	Electrical Discharge Machining
H-M-P	Hybrid Machining Process
RSM	Response Surface Methodology
DC	Duty Cycle (%)
DF	Dielectric Fluid
I	Ampere-Current (Ampere)
MRR	Rate of Material Removal (mm^3/minute)
SR	Surface Roughness (μm)
RPM	Revolution per minute
WS	Wheel Speed (RPM)
T_{on}	Pulse-on-time (μs)
T_{off}	Off-time of pulse
T	Time in minute
P	Density of work-piece material ($gram/cm^3$)
Ra	Average Surface Roughness (μm)
WMPI	Weighted Multiple Performance Index
WPCA	Weighted Principal Component Analysis
IEG	Inter Electrode Gap
Cr	Chromium
GRA	Grey Relational Analysis
TM	Taguchi Method
N % Probability	Normal Percentage Probability
PC/PCs	Principal Component/Principal Components

GRC	Grey Relational Coefficients
WRLT	White Recast Layer Thickness
SEM	Scanning Electron Microscopy
WEDM	Wire EDM
S-DG	Surface Diamond Grinding
ED-M/ED-Machining	Electrical Discharge Machining
EDDSG	Electrical Discharge Diamond Surface Grindimg
GRA-PCA	Grey Relational Analysis-Principal Component Analysis
MMCs	Metal Matrix Composites
MMMCs	Hybrid Metal Matrix Composites
O-A	Orthogonal Array